ORIGINAL RESEARCH PAPER

Fuel Cells DOI: 10.1002/fuce.201000085

Synthesis and Properties of Segmented Block Copolymers of Functionalised Polybenzimidazoles for High-Temperature PEM Fuel Cells

J. A. Mader[1] and B. C. Benicewicz[1]*

[1] Department of Chemistry and Biochemistry and USC Nanocenter, University of South Carolina, 631 Sumter St., Columbia, SC 29208, USA

Received May 16, 2010; accepted December 26, 2010

Abstract

A series of novel segmented block copolymers of sulphonated polybenzimidazole (PBI) (s-PBI) and *p*-PBI were prepared with various polymer ratios (10–90 mol% s-PBI; 90-10 mol% *p*-PBI). A two-step synthesis of oligomeric species, followed by combination and further polymerisation was used via the polyphosphoric acid (PPA) process. The membranes showed improved high-temperature proton conductivities and fuel cell performance over previous literature reports, with moderate incorporation of s-PBI into the copolymer showing the best results. The non-humidified fuel cell performance was extensively studied with various fuels and oxidants and showed excellent properties. Block copolymers that incorporated 40, 50 or 60 mol% s-PBI and the corresponding 60, 50 or 40 mol% *p*-PBI, at 0.2 A cm^{-2} and 160 °C, had hydrogen–air performances of 0.661–0.666 V, depending on composition. The performance was improved using hydrogen–oxygen, with voltages between 0.734 and 0.742 V at 0.2 A cm^{-2} and 160 °C. Fuel cells operating on a reformed hydrocarbon gas showed decreased performance (0.622–0.627 V, same conditions), especially at lower temperatures, but was significantly improved over previous literature reports of sulphonated PBI membranes operating at high temperatures.

Keywords: Fuel Cell, High-Temperature Polymer Electrolyte Membrane, PPA Process, Segmented Block Copolymers of PBI, Sulphonated Polybenzimidazole

1 Introduction

Solid polymer electrolytes for fuel cell applications have gained much attention recently as a promising technology to meet today's energy needs [1]. These are especially attractive because fuel cells are clean energy devices, eliminating many of the atmospheric pollutants produced from conventional energy production methods. The membrane functions in several different roles in the fuel cell. In addition to transporting protons, the polymer electrolyte must have the following capabilities: high-proton conductivity, low gas permeability (prevent crossover of fuel and oxidant), electrical insulator (prevent short circuiting), good mechanical properties, thermal and chemical stability and low cost. Typically, the main focus on fuel cell membranes has been on perflurosulphonic acid (PFSA)-based membranes, such as Nafion®. The proton conductivities of PFSA membranes are highly dependent on water content [2]. The dependence on water for proton conduction is one of the main drawbacks of this type of fuel cell operation, and thus, water management continues to be one of the most critical issues facing water-based fuel cell systems. Because water molecules are transported through the membrane with each proton (electro-osmotic drag), the fuel gas needs to be humidified to replenish the membrane water. Additionally, the operating temperatures need to be maintained below 100 °C and practical operation is limited to

[*] *Corresponding author, benice@sc.edu*

80 °C to avoid membrane drying. However, system engineering solutions, such as operating the fuel cell under pressure, allow this temperature limitation to be overcome. At the same time, water on the cathode side (from proton transport and reaction product) needs to be removed quickly to avoid flooding the electrode and blocking the catalyst. Furthermore, the lower temperature of typical operation (≤80 °C) leaves the cell susceptible to catalyst poisoning by fuel impurities, loss of proton conductors (i.e. water), slower reaction kinetics and complex water management and radiator systems.

If new membranes were developed that could operate at higher temperatures, many of these problems would be alleviated. The benefits of higher temperatures include: faster reaction kinetics at the electrodes, simplified water management, simplified cooling system, increased tolerance to fuel impurities (CO) and better utilisation of generated heat (cogeneration of heat and power) [3]. The increased tolerance to fuel impurities is especially attractive, as it widens the field of fuel choices and lowers fuel reforming costs. These reasons have placed a major emphasis on developing high-temperature (>100 °C) fuel cell membranes. To combat the high cost of PFSA membranes and their susceptibility to degradation, there has been much investigation into sulphonated hydrocarbon alternative polymers. Sulphonated aromatic polymers such as polyimides [4, 5], polysulphones [6], polybenzoxazoles [7], poly(ether ether ketones) [8–11], poly(arylene ether)s [12–14], poly(benzobisthiazole)s [15], polyphosphazenes [16–18] and poly(phenylene sulfide) [19], among others, have been widely investigated for this type of application. Additionally, many copolymers and polymer blends have been investigated, and are reviewed nicely in the literature [14, 20]. However, these membranes still rely on water as the proton conduction medium. To avoid the challenges associated with water, membranes based on acid–base complexes have been developed [21–25]. Typically, the polymer backbone has a strong basic site such as an ether, alcohol, imine, amide or imide group and can react strongly with acids. Among the polymers investigated were poly(ethylene oxide) (PEO) [26], poly(vinyl acetate) (PVA) [27], polyacrylamide (PAAM) [28–30], poly(ethyleneimine) (PEI) [31] and polybenzimidazole (PBI) [32–41]. In these cases, phosphoric acid (PA) is typically used as the proton conductor due to its thermal stability and high-proton conductivity at high temperature. Other investigations with heteropolyacids (phosphotungstic acid, zirconium phosphate and silicotungstic acid) in various polymers have also been pursued [25, 42]. The most successful of these alternative polymers is the PA-doped PBI. PA-doped PBI was first introduced in 1995 by Wainright et al. [35] as a new class of polymer electrolyte capable of operating in high-temperature fuel cells (>120 °C). Following this initial report, there has been much work devoted to developing PA-doped PBI membranes, and has been reviewed recently [34]. The advantages of a PBI/acid-based high-temperature PEM fuel cell include: (1) operation up to 200 °C, (2) reduction or elimination of water management, (3) excellent thermal and chemical stability, (4) nearly zero water drag coefficient and (5) significantly lower cost of PBI membranes. Conventional methods to prepare PA-doped PBI membranes are typically as follows: (1) casting from a DMAc/LiCl solution, then imbibing the film in a PA bath [34, 35, 43, 44] or (2) casting of PA-doped PBI membranes from a solution of trifluoroacetic acid (TFA) and PA [45]. The acid doping levels of these films are typically 5–10 moles of PA per mole polymer repeat unit (mol PA/PRU), and proton conductivities are 0.01–0.04 S cm^{-1} at 130–190 °C [46]. The direct cast TFA/PA films showed increased conductivities of 0.04–0.08 S cm^{-1}, but had weak mechanical properties. While these values are low compared to Nafion®, they are measured at temperatures where conventional PFSA fuel cell membranes cannot operate without additional engineering solutions. The initial report of PA-doped PBI demonstrated fuel cell performance with hydrogen and methanol as fuels and oxygen as an oxidant [35]. A separate report also described fuel cell performance with hydrogen–oxygen [47] and details of the MEA fabrication. The fuel cell was able to operate for over 200 h at 150 °C a constant cell voltage of 0.55 V without membrane dehydration or failure. More recent improvements and overall performance were reviewed recently [34]. Some of the perceived drawbacks of the PA-doped PBI membranes are low PA loading levels (<10 mol PA/PRU), low proton conductivity with respect to high-temperature liquid PA-based fuel cells (<0.1 S cm^{-1}), poor mechanical properties, low molecular weight of the polymer and the multistep doped film formation process.

Recently, a novel method of synthesising high-molecular weight PBI polymers and casting films was developed [32, 33, 36–41]. This method, termed the PPA process, eliminates many of the problems associated with the conventional procedures. The PPA process allows for a single step polymerisation/casting procedure to produce high-molecular weight (high-inherent viscosity; IV) PBI polymers with high-proton conductivities, excellent mechanical properties and high-acid doping levels (>20 mol PA/PRU). The Polyphosphoric acid (PPA) Process uses PPA as both the polycondensation agent and casting solvent for synthesis of PBI. The polymer was synthesised directly in PPA solution and then the PPA solution was cast directly onto clean glass plates at 220 °C. No organic solvents are required during this process because there is no polymer isolation and redissolution. A variety of PBI derivatives have been prepared via the PPA process and studied extensively to determine the relationships between the chemical structure of the PBI and important fuel cell properties such as acid loading, conductivity, mechanical properties and fuel cell performance [32, 33, 36–41]. It was found that the chemical structure of the PBI repeat unit greatly affects the fuel cell properties of the membranes.

It is well known that polymer architecture has an influence on final polymer properties. Previous work has focused on the development of a sulphonated PBI homopolymer [40] and random copolymers of sulphonated PBI and *p*-PBI [41]. The work in this paper focuses on developing and characterising a series of segmented block copolymers of sulphonated

PBI and *p*-PBI. These polymers combine the chemistry of low temperature membranes (sulphonic acid groups) with the stability and high temperature performance capabilities of acid-doped PBI membranes. By varying the ratio of the polymers, an extensive study into the structure–property relationships of these membranes was carried out. Fuel cell performance with various fuels and oxidants was investigated as a key indicator of the practical applications of these membranes.

2 Experimental Part

2.1 Materials

Celanese Ventures, GmbH donated 3,3′,4,4′-tetraaminobiphenyl (TAB, polymerisation grade) and it was used as supplied. Terephthalic acid (TPA, 99+%) was purchased from Amoco and used as received. The monosodium salt of 2-sulphoterephthalic acid (s-TPA, 98%) was purchased from TCI America and dried in a vacuum oven overnight at 120 °C prior to use. PPA (115%) was used as supplied from Aldrich Chemical Company and FMC Corporation. PA (85%) was purchased from Fisher Scientific and used as received.

2.2 Preparation of Segmented Block Copolymers

The general approach for the preparation of segmented block copolymers began with separate syntheses of oligomeric species of each polymer block, followed by their combination and continued polymerisation. Scheme 1 depicts the synthesis of the s-PBI-*b*–*p*-PBI copolymers. Prepolymers of s-PBI (**1**) and *p*-PBI (**2**) were synthesised in PPA in separate reactions using temperature and time profiles intended to give low molecular weight (low IV) polymers. Following prepolymerisation, solutions of **1** and **2** were mixed and polymerised further in controlled molar ratios to prepare segmented block copolymers. A number of compositions of the segmented block copolymers were synthesised to investigate the effect of copolymer composition on polymer and membrane properties. The copolymers were prepared with molar ratios of s-PBI to *p*-PBI units (*x*:1 – *x* in Scheme 1) of 90:10, 80:20, 75:25, 60:40, 50:50, 40:60, 25:75, 20:80 and 10:90.

2.2.1 s-PBI Prepolymer

TAB (2.1427 g, 10 mmol) and 2-sulphoterephthalic acid, monosodium salt (s-TPA, dried before use) (2.6818 g, 10 mmol) were added to a 100 mL three neck reaction flask in a nitrogen glovebox. PPA (106.79 g) was added for a final prepolymer concentration of 3.5 wt% solids. The PPA solution was stirred under a slow nitrogen purge with an overhead mechanical stirrer. The reaction temperature was controlled via a programmable temperature controller with ramp (increasing to a specified temperature over a specified time period) and soak (maintaining the specified temperature for the specified time) capability. The polymerisation scheme is described below:

Temperature profile: 150 °C–ramp: 1 h, soak: 2 h; 170 °C–ramp: 0.5 h, soak: 2 h; 195 °C–ramp: 0.5 h, soak: 4 h.

A small amount of solution was removed from the reactor for polymer characterisation. The typical IV of the prepolymer was 0.74 dL g^{-1}. This slightly higher molecular weight was chosen for the s-PBI prepolymer due to poor properties and film formation at lower molecular weights.

2.2.2 p-PBI Prepolymer

TAB (2.143 g, 10 mmol) and TPA (1.661 g, 10 mmol) were added to a 100 mL three neck reaction flask in a nitrogen glo-

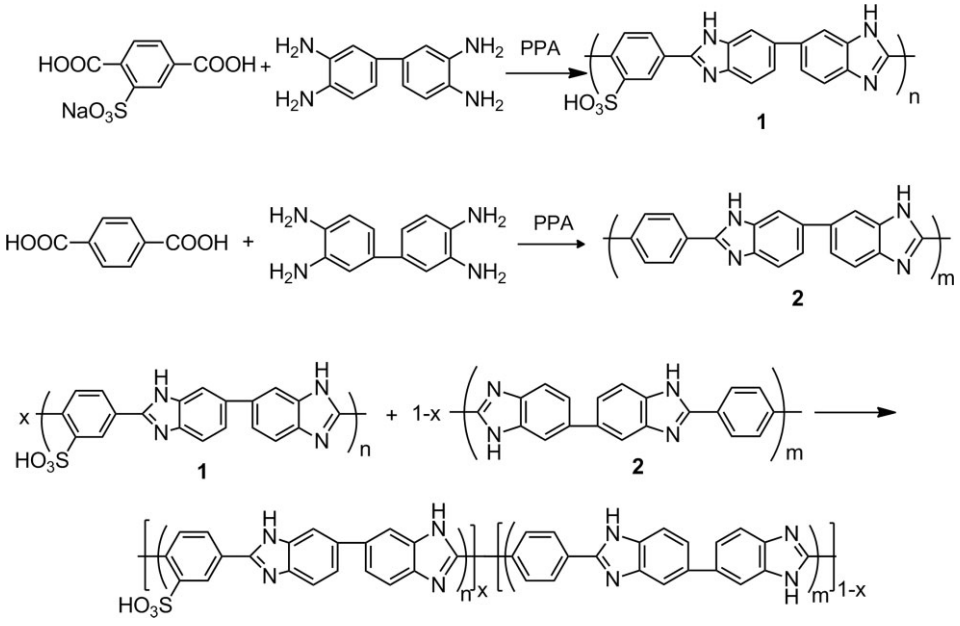

Scheme 1 Synthesis of s-PBI/*p*-PBI segmented block copolymers.

vebox. PPA (101.18 g) was added for a final prepolymer concentration of 3.0 wt% solids. The PPA solution was stirred under a slow nitrogen purge with an overhead mechanical stirrer. The reaction temperature was controlled via a programmable temperature controller. The polymerisation scheme is described below:

Temperature profile: 120 °C– ramp: 0.25 h, soak: 0.5 h; 140 °C–ramp: 0.5 h, soak: 1 h; 160 °C–ramp: 0.5 h, soak: 1 h; 180 °C–ramp: 0.5 h, soak: 1.75 h.

A small amount of solution was removed from the reactor for polymer characterisation. The typical IV of the prepolymer was 0.22 dL g^{-1}.

2.2.3 Polymerisation of Segmented Block Copolymers

After the s-PBI and *p*-PBI prepolymers were prepared, the solutions were mixed together in a separate 300 mL reactor, according to the calculated molar ratios. The prepolymers of s-PBI used in all segmented block copolymerisations all had IV's of ~0.74 dL g^{-1}, while all the *p*-PBI prepolymers had an IV of ~0.22 dL g^{-1}. In other words, the block lengths were kept consistent across all polymerisations, and only the molar ratios of s-PBI and *p*-PBI were varied. The prepolymer mixture was polymerised further as described below:

Temperature profile: 180 °C–ramp: 0.25 h, soak 4.25 h; 220 °C–ramp: 2.5 h, soak 8–11 h.

The polymerisation was conducted until a significant Weissenberg effect was observed. At this point, the polymerisation was stopped and 10 mL of 85% PA was added to the reaction flask and allowed to stir for 30 min for complete integration. The final polymer solids concentrations were determined by titration and ranged from 4.5 to 6.22 wt%, depending on composition. Polymer IV's were composition dependent and were 1.61–3.26 dL g^{-1}.

2.2.4 Membrane Preparation

Segmented block copolymer films were prepared by direct casting of the hot (220 °C) polymer solution onto clean glass plates using a Gardner doctor blade. Casting thicknesses were typically 15–25 mils (381–635 µm). After casting, the films were placed in a controlled humidity chamber at relative humidity (RH) = 55 ± 5% and room temperature for 24 h to hydrolyse the PPA to PA and induce a sol–gel transition. PA-doped gel membranes were formed during this process.

2.3 Polymer and Membrane Characterisation

2.3.1 Inherent Viscosity

A small amount of each prepolymer and segmented block copolymer solution was precipitated in distilled water. The polymer was pulverised and neutralised with ammonium hydroxide. The polymer powder was then filtered, washed with distilled water until neutral and to remove any salts, then dried under vacuum at 110 °C for 24 h. The dried powder was dissolved in concentrated sulphuric acid (96%) at a concentration of 0.2 dL g^{-1}. The inherent viscosities were measured using Canon Ubbelohde viscometers at 30.0 °C.

2.3.2 Phosphoric Acid Content

PA content was measured by titration of a small sample of membrane with standardised 0.1 N sodium hydroxide solution. Samples of the membrane were cut, weighed and placed in a 100 mL beaker with 50 mL of distilled water. The samples were stirred with gentle heating for 30 min to extract PA, then titrated using a Metrohm 716 DMS Titrino autotritrator. After titration, the film was dried under vacuum at 110 °C overnight and weighed to obtain the dry sample weight for solids content determination. The PA doping level in moles of PA per mole of polymer repeat unit (mol PA/PRU) was calculated from Eq. (1):

$$\text{PA doping level } X = (V_{\text{NaCH}} \times C_{\text{NaOH}})/(W_{\text{dry}}/M_{\text{w}}) \quad (1)$$

Where V_{NaOH} and C_{NaOH} are the volume and normal concentration of the sodium hydroxide titer, W_{dry} the dry polymer sample weight and M_{w} is the average molecular weight of the repeat unit containing both s-PBI and *p*-PBI in their actual molar ratios.

2.3.3 Ionic Conductivity

Proton conductivity was measured by four-probe AC impedance spectroscopy with a Zahner IM6e impedance spectrometer in the frequency range of 1 Hz–100 KHz. Two conductivity runs in air were performed. In the first run, the temperature was increased to 180 °C in 20° intervals to remove water, with subsequent cooling under vacuum before performing a second run. The temperature during the second run was increased to 180 °C in 20° intervals, and held at 180 °C for 5 h. Before measurement at each temperature setpoint, the samples were held at constant temperature for at least 15 min for thermal equilibration. Typically, system thermal equilibrium was reached within 1 min due to the small thermal mass being tested. For the measurement of conductivity at constant temperature (Figure 1b), the membrane sample was held at 180 °C following the second heating run and proton conductivity was recorded continuously with time during the remaining portion of the experiment. A two-component model with a resistor in parallel with a capacitor was used to fit the experimental data of membrane resistance across the frequency range. The proton conductivity was calculated from room temperature to 180 °C using Eq. (2):

$$\sigma = \frac{D}{L \cdot W \cdot R} \quad (2)$$

where D is the distance between the two current electrodes, L and W are the thickness and width, respectively and R is the measured resistance value. The distance between the sensor

ORIGINAL RESEARCH PAPER

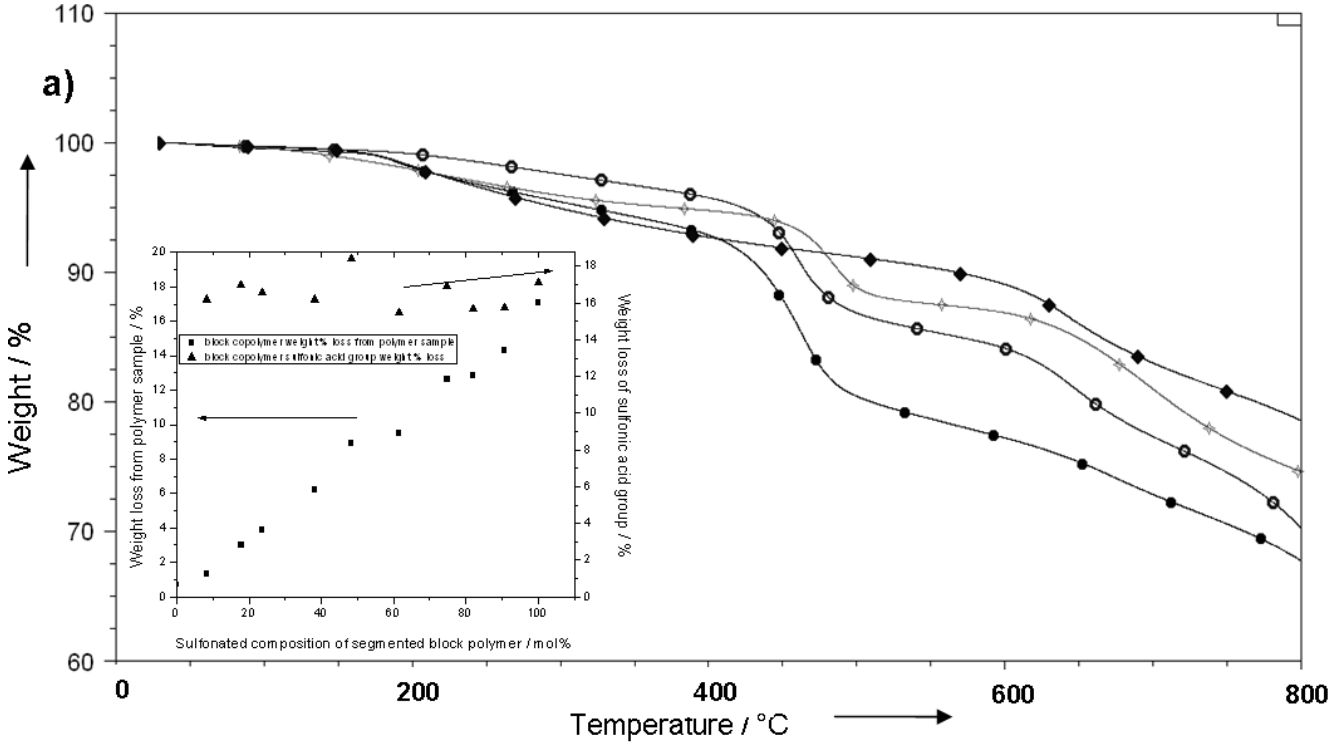

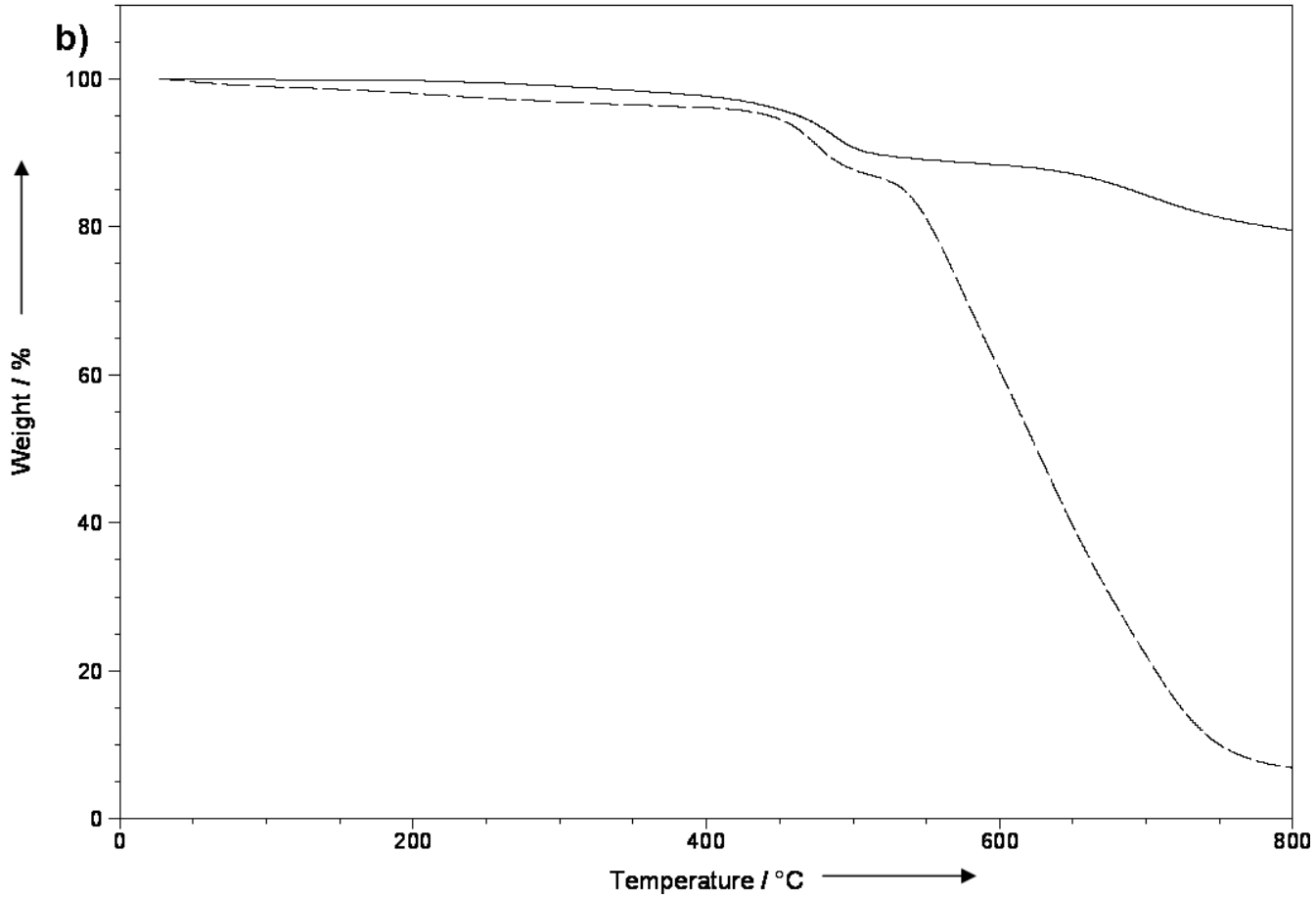

Fig. 1 (a) TGA in nitrogen of *p*-PBI and representative examples of segmented block copolymers (90/10 s-PBI/*p*-PBI, closed circles; 60/40 s-PBI/*p*-PBI, open circles; 40/60 s-PBI/*p*-PBI, open diamonds; *p*-PBI, closed diamonds) and relationship between s-PBI content and weight loss over 425–525 °C (inset); (b) TGA in nitrogen (solid line) and air (dashed line) of a representative block copolymer (50/50 s-PBI/*p*-PBI).

and test electrodes was 2.0 cm. The temperature range investigated was room temperature to 180 °C.

2.3.4 Mechanical Properties

According to ASTM D638 specifications, Type V specimens were cut. The tensile properties of the segmented block copolymers were measured in atmospheric conditions using an Instron Model 5846 system with a 100 N load cell and crosshead speed of 10 mm min^{-1} or an Instron Model 5543A system with a 10 N load cell and crosshead speed of 5 mm min^{-1}. Samples were preloaded to 0.1 N. No differences were seen between the different crosshead speeds and final properties were in agreement between the instruments.

2.3.5 Thermogravimetric Analysis (TGA) and Infrared Spectroscopy

The thermal stability and thermal oxidative stability of the polymers was determined by TGA performed on dried polymer samples from room temperature to 800 °C using a TA Instruments Q5000 with a nitrogen or air flow rate of 25 mL min^{-1} and heating rate of 10 °C min^{-1}. Attenuated total reflectance (ATR) infrared spectra were obtained using a Perkin-Elmer Spectrum 100 FT-IR with a three-reflection diamond/ZnSe crystal. Spectroscopy was performed on both dried powder and dried films in the range of 4 000–650 cm^{-1}.

2.3.6 Fuel Cell Performance

Fuel cell performance was measured using 50 cm^2 single cell stacks (active area: 45.15 cm^2). The membrane electrode assembly (MEA) was prepared by hot pressing the acid-doped membrane between an anode electrode and a cathode electrode at 140 °C and 30–40 s at 4.45 MPa. The MEA was shimmed for a 20% target compression from the original MEA thickness. Electrodes were received from BASF Fuel Cell, Inc. and used without additional manipulation (e.g. addition of PA). Anode electrodes contained only Pt as the catalyst (1.0 mg cm^{-2}), while the cathode electrodes contained a BASF Fuel Cell standard cathode Pt alloy (0.7 mg cm^{-2} Pt). Polarisation curves were obtained from 120 to 180 °C with hydrogen or reformate fuels and air or oxygen oxidants with no gas humidification. Long-term durability tests were conducted at 160 °C at a constant current of 0.2 A cm^{-2} with non-humidified hydrogen and air at ambient pressure.

3 Results and Discussion

3.1 Synthesis and Characterisation of the s-PBI/p-PBI Segmented Block Copolymers

The s-PBI oligomer was polymerised to an IV of ~0.74 dL g^{-1} in order to allow sufficient mechanical properties for film formation. The *p*-PBI block was polymerised to an average IV ~0.22 dL g^{-1}. Segmented block copolymerisations with s-PBI oligomer IV's <0.50 dL g^{-1} and/or *p*-PBI oligomer IV's <0.12 dL g^{-1} did not form high IV copolymer, as evidenced by low viscosity solutions and polymer precipitation out of solution after casting and hydrolysis. The final segmented block copolymer IV was generally dependent on s-PBI composition, as seen in Table 1, with s-PBI and *p*-PBI homopolymers included for comparison. The segmented block copolymers produced were high-molecular weight (>1.0 dL g^{-1}).

Polymer characterisation of structure and stability included Fourier transform infrared spectroscopy (FT-IR) and TGA. Triple pass ATR infrared spectroscopy was used to confirm the incorporation of the sulphonated PBI polymer into the overall block copolymer structure. The spectra were similar to those described for the random copolymers of s-PBI and *p*-PBI [41]. The major SO bands seen in the IR were at 800 cm^{-1} due to the symmetric S–O stretch, 1 019–1 022 cm^{-1} and 1 070 cm^{-1} from the S=O symmetric stretches and 1 167–1 172 and 1 222 cm^{-1} due to asymmetric stretching of S=O. The peak at 1 623 cm^{-1} was characteristic of the C=C/C=N stretching vibrations in the imidazole. The absence of a strong band in the 1 650–1 780 cm^{-1} region indicates complete closure of the imidazole ring. The SO bands were in agreement with the literature [40, 48–50] and were not seen in the *p*-PBI homopolymer spectrum, indicating the incorporation of the s-PBI polymer and stability of the sulphonic acid moiety during polymer synthesis and work up.

TGA was performed to determine the thermal stability and thermal oxidative stability of the segmented block copolymers at fuel cell operating temperatures (120–180 °C), and selected results for some of the segmented block copolymers are shown in Figure 1. Figure 1a shows the TGA of the polymers in nitrogen, while Figure 1b shows a representative block copolymer sample (50/50 s-PBI/*p*-PBI) in nitrogen and air. The decomposition of the sulphonic acid group began at ~425 °C for all block copolymers in both nitrogen and air, as seen in the literature [40, 49–58] for sulphonated hydrocarbon polymers. The *p*-PBI trace does not show a large weight loss

Table 1 s-PBI/*p*-PBI segmented block copolymer properties.

Membrane type	Sulph. Comp.[a]	Solids content / wt%[b]	IV / dL g^{-1}	PA loading / mol PA/PRU	Conductivity at 180 °C / S cm^{-1}
s-PBI	100.00	3.42	1.86	40.0	0.099
90/10 s/*p*-PBI seg block	90.76	5.87	1.61	37.0	0.18
80/20 s/*p*-PBI seg block	81.90	6.22	1.87	34.2	0.23
75/25 s/*p*-PBI seg block	74.79	4.82	2.45	56.2	0.34
60/40 s/*p*-PBI seg block	61.44	5.57	2.34	36.8	0.34
50/50 s/*p*-PBI seg block	48.32	4.82	2.85	56.6	0.33
40/60 s/*p*-PBI seg block	38.26	4.54	2.60	42.8	0.34
25/75 s/*p*-PBI seg block	23.54	4.49	3.18	61.4	0.38
20/80 s/*p*-PBI seg block	17.80	5.85	2.62	33.2	0.26
10/90 s/*p*-PBI seg block	8.22	6.02	3.26	30.4	0.34
p-PBI	0.00	2.86	3.66	61.7	0.28

[a] Exact molar s-PBI composition in segmented block copolymer. *p*-PBI content is 100% minus s-PBI content.
[b] Polymer film solids determined from titration calculations.

at this temperature, indicating that this is the decomposition of the sulphonic acid functionality. The decomposition temperature is well above the desired operating temperature for fuel cells and excellent stability is seen up to 200 °C in both nitrogen and air, indicating both thermal and thermal oxidative stability. The small weight losses below this temperature were attributed to water absorbed from the atmosphere, due to the hygroscopic nature of PBI polymers in general, and was also seen in the *p*-PBI sample.

The copolymer sample weight loss in nitrogen over 425–525 °C increased linearly with increasing s-PBI content in the block copolymer, while the amount of sulphonic acid group decomposition remained independent of copolymer composition at ~17 wt% (Figure 1a inset). The sulphonic acid group comprises 20.91 wt% of the s-PBI block, so the lower decomposition values indicate the desulphonation step is not complete over the temperature range. It was found that the 10/90 s-PBI/*p*-PBI copolymer had the smallest decomposition over this range (1.329 wt% of sample, 16.17 wt% of sulphonic acid group) and the 90/10 s-PBI/*p*-PBI copolymer had the largest losses (14.28 wt% sample, 17.097 wt% sulphonic acid group).

NMR and elemental analysis were performed on the block copolymers, but the obtained data were not meaningful. NMR characterisation of PBIs prepared with *para*-oriented phenyl rings (rather than the typical *meta*-orientation) is difficult due to the extreme insolubility of these polymers in typical organic solvents (e.g. dimethylacetamide). At low polymer concentrations, concentrated sulphuric acid was found to dissolve these polymers. However, the corresponding NMR spectra (in D_2SO_4) were extremely unclear and interpretation was not possible. In the literature, there have been many reports of the high-thermal stability of wholly aromatic PBIs, even at extremely high temperatures in air. Thus, achieving accurate elemental analysis data is challenging.

3.2 Film Formation

Acid-doped films of both s-PBI and *p*-PBI homopolymers have been previously produced by the PPA process [39, 40]. The segmented block copolymers were successfully prepared via prepolymerisation of oligomeric species followed by combination and further polymerisation to produce high-MW (IV >1.0 dL g^{-1}) polymers with controlled s-PBI/*p*-PBI ratios. All segmented block copolymers formed robust orange–red translucent gel films under appropriate casting and hydrolysis conditions. This occurs because (hot) PPA is a good solvent for PBI (sol state), while room temperature PA is a poor solvent (gel state), as previously reported. For all block copolymer compositions, the gel state remained stable even on reheating to fuel cell operating temperatures (120–180 °C).

3.3 Membrane Properties

3.3.1 Membrane Doping Levels and Proton Conductivity

Acid doping levels of the copolymer membranes were determined by titration with standardised 0.1 N sodium hydroxide solution. The PA loading (mol PA/PRU) was calculated using the average molecular weight of the repeat unit containing s-PBI and *p*-PBI in their actual molar ratios. The titration results are reported in Table 1. In general, PA loading was not affected by copolymer composition, likely due to the gel nature of the films. The films contained similar solids content (4.5–6.2 wt%), regardless of composition, meaning the remainder of the weight is composed of PA and a small amount of water. Most of the segmented block copolymers retained 30–40 mol PA/PRU, but the 25/75, 50/50 and 75/25 s-PBI/*p*-PBI block copolymers had loading levels of ~60 mol PA/PRU. The ionic conductivities of the block copolymers compared to s-PBI and *p*-PBI are shown in Figure 2.

All membranes showed excellent conductivities (>0.1 S cm^{-1}) at elevated temperatures with no humidification. The conductivities of the block copolymers were significantly higher than the s-PBI homopolymer at all temperatures and compositions tested, even with similar acid loading levels. There is little dependence of conductivity on acid doping level within the ranges tested, especially for the 30–40 mol PA/PRU doping levels. In previous work [59], a direct correlation has been shown for the conductivity of a specific PBI membrane with increasing PA loading. In general, as PA loading increases, conductivity increases until a plateau is reached. At this point (~60 mol PA/PRU), so much PA is available for conduction that not all PA molecules are used in the proposed 'hopping' mechanism. However, the exact mechanism of proton conduction is unknown, especially for these new polymer chemistries in an acid-based system, so the relative contribution of the PA *versus* the sulphonic acid/imidazole moieties is unknown. In this case, a slight increase in conductivity was seen for the highest doping levels (~ 60 mol PA/PRU), but could also be due to copolymer composition. The highest conductivity was found for the 25/75 s-PBI/*p*-PBI membrane (0.376 S cm^{-1}), with an acid loading of 61.44 mol PA/PRU, while the lowest conductivity was found for the 90/10 s-PBI/*p*-PBI membrane (0.181 S cm^{-1}), with an acid loading of 36.95 mol PA/PRU. In general, adding moderate amounts of s-PBI (25–75 mol%) into the copolymer increased the conductivity above the s-PBI or *p*-PBI homopolymer (>0.28 S cm^{-1}), while either very high or low s-PBI content lowered the conductivity (90, 80 and 20 mol%), though the 10/90 s-PBI/*p*-PBI showed an anomalously high conductivity at relatively low acid doping level (30 mol PA/PRU), perhaps due to a morphological rearrangement of the copolymer due to low s-PBI content. From these data, we observe a general trend that when we have a high amount of block copolymer-type morphology, such as in the 40–60/60–40 mol% compositions, conductivity is enhanced, while a low amount of block copolymer morphology, such as in the 10/90 or 90/10 compositions, is unable to improve conductivity. The acid doping levels and conductivities are all significantly higher than previous literature reports for sulphonated PBI membranes, including random copolymers (10^{-6}–10^{-1} S cm^{-1}) [40, 41, 48–54, 56, 58, 60–64].

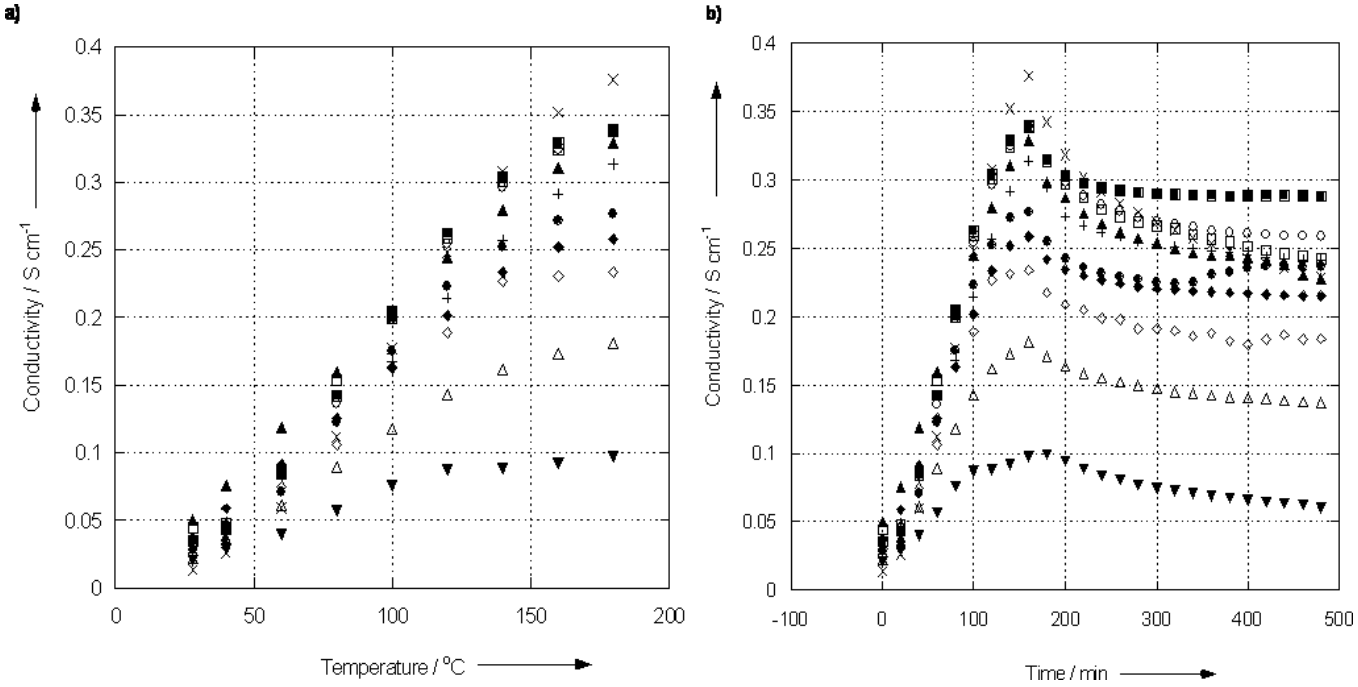

Fig. 2 Ionic conductivities of s-PBI (▼, 40 mol PA/PRU), 90/10 s-PBI/*p*-PBI segmented block copolymer (△, 37 mol PA/PRU), 80/20 s-PBI/*p*-PBI segmented block copolymer (◇, 34 mol PA/PRU), 75/25 s-PBI/*p*-PBI segmented block copolymer (□, 56 mol PA/PRU), 60/40 s-PBI/*p*-PBI segmented block copolymer (○, 37 mol PA/PRU), 50/50 s-PBI/*p*-PBI segmented block copolymer (▲, 57 mol PA/PRU), 40/60 s-PBI/*p*-PBI segmented block copolymer (+, 43 mol PA/PRU), 25/75 s-PBI/*p*-PBI segmented block copolymer (x, 61 mol PA/PRU), 20/80 s-PBI/*p*-PBI segmented block copolymer (◆, 33 mol PA/PRU), 10/90 s-PBI/*p*-PBI segmented block copolymer (■, 30 mol PA/PBI) and *p*-PBI (●, 62 mol PA/PRU) *vs.* (a)temperature and (b) time.

3.3.2 *Mechanical Properties*

The mechanical properties of the segmented block copolymers were investigated to determine composition effects. After hydrolysis, the membranes contained between 4.5 and 6.22 wt% solids and 95.5–93.78 wt% PA and water. The polymer membranes synthesised via the PPA process are characterised as non-crosslinked polymer gels, or Flory Type III gels. Due to the composition and nature of a gel film (low solids, high liquid), mechanical properties are expected to be lower than the fully dense films produced from organic solvents. Table 2 and Figure 3 show the mechanical testing characteristics and stress–strain curves, respectively.

A general trend was observed that the tensile stress at break increased with greater p-PBI content in the block copolymer. The highest tensile stress at break (4.830 MPa) and second highest tensile strain (566%) were seen for the 25/75 s-PBI/*p*-PBI segmented block copolymer, while the lowest mechanical properties were observed from the 40/60 s-PBI/*p*-PBI segmented block copolymer. The lower mechanical properties for some of the block copolymers may be due to the molecular weight of the polymer. Because the IV's of the block copolymers were dependent on s-PBI content and prepolymer IV, this may contribute to poorer mechanical properties even with higher *p*-PBI content. Additionally, because the membranes are hand-cast, a variation in mechanical properties would be expected, especially since the true morphologies of these gel membranes has not yet been studied extensively. The incorporation of even a small amount of *p*-PBI into the block copolymer improved mechanical properties over the s-PBI homopolymer. All membranes were able to undergo MEA fabrication and fuel cell testing, indicating the robust mechanical properties of the s-PBI/*p*-PBI block copolymers.

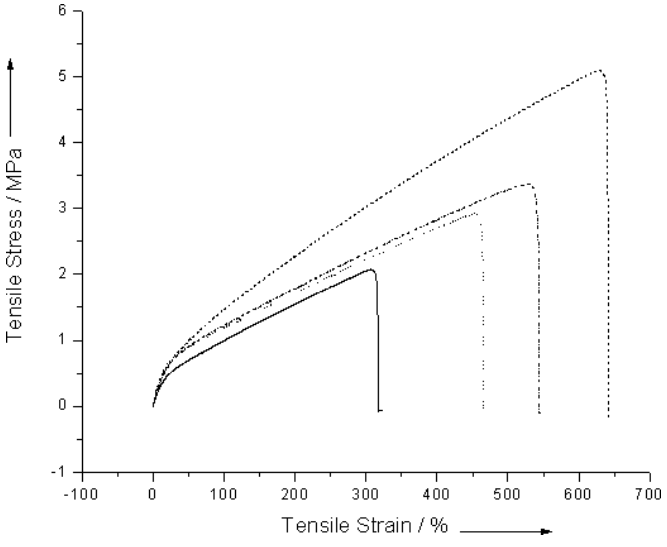

Fig. 3 Tensile stress–strain curves of 10/90 s-PBI/*p*-PBI segmented block copolymer (dashed line, - - -), 25/75 s-PBI/*p*-PBI segmented block copolymer (dash-dot line, - - -), 20/80 s-PBI/*p*-PBI segmented block copolymer (dotted line, ·····), 50/50 s-PBI/*p*-PBI segmented block copolymer (solid line, -).

Table 2 Mechanical testing results for s-PBI/*p*-PBI segmented block copolymers.

Type	Modulus / MPa	Average tensile stress at break / MPa	Average tensile strain at break /%
s-PBI homopolymer	2.52	1.56	160
90/10 s-PBI /p-PBI seg block	1.93	2.45	264
80/20 s-PBI /p-PBI seg block	1.49	1.97	416
75/25 s-PBI /p-PBI seg block	1.67	2.02	248
60/40 s-PBI /p-PBI seg block	0.780	2.44	467
50/50 s-PBI /p-PBI seg block	1.19	1.99	295
40/60 s-PBI /p-PBI seg block	1.42	1.36	287
25/75 s-PBI /p-PBI seg block	1.34	4.83	566
20/80 s-PBI /p-PBI seg block	1.13	2.94	446
10/90 s-PBI /p-PBI seg block	0.961	3.54	592

3.4 Fuel Cell Performance

Fuel cell performance was measured on 50 cm^2 (active area: 45.15 cm^2) single cells. The fuel (hydrogen or reformate) and oxidant (air or oxygen) gases were supplied at stoichiometries of 1.2 and 2.0, respectively, without humidification. The reformate gas had a composition of 70% hydrogen, 28% CO_2 and 2% CO (impurity). Polarisation curves were obtained from the various fuel and oxidant gases from 120 to 180 °C. Long-term durability studies were performed at 160 °C at a constant current of 0.2 A cm^{-2} with hydrogen and air. The fuel cell performance was examined for each membrane composition, and it was found that moderate incorporation of s-PBI (40–60 mol%) into the segmented block copolymers yielded the best polymer and fuel cell properties. The following performance discussions will focus on these polymers.

3.4.1 Hydrogen–Air and Long-Term Performance

The hydrogen–air fuel cell performance of the segmented block copolymers at 0.2 A cm^{-2} is summarised in Figure 4a. Fuel cell performance was temperature-dependent, as would be expected from the predictions of the Nernst Equation. The relationship between temperature and the voltage gain (ΔV_T) for PA fuel cell systems (PAFC's) suggested from experimental data with hydrogen–air is summarised by Eq. (3):

$$\Delta V_T = 1.15\,(T_2 - T_1)\,\text{mV} \qquad (3)$$

in the temperature range of 180 °C <T<250 °C [65, 66]. Performance with hydrogen–air was extremely robust at all temperatures tested with dry gases (Figure 5), as opposed to typical PFSA membranes and some acid-doped PBI membranes in the literature which require humidification. The lowest voltage increases using hydrogen and air were seen for 50/50 and 60/40 s-PBI/p-PBI block copolymer membrane compositions (0.96 and 1.05 mV $°C^{-1}$, respectively), while the 40/60 s-PBI/*p*-PBI block copolymer showed an increase of 1.24 mV $°C^{-1}$. Considering the significantly lower operating temperatures of the PEMFC compared to those described in Eq. (3), these values are in general agreement with the literature. The maximum performance (0.666 V at 0.2 A cm^{-2}, 160 °C) was seen for the 60/40 s-PBI/*p*-PBI block copolymer, followed closely by the 50/50 s-PBI/*p*-PBI block copolymer (0.665 V, same conditions). The 40/60 s-PBI/*p*-PBI block copolymer showed a slightly lower performance of 0.661 V under the same conditions. These values are greatly improved over those reported for the s-PBI homopolymer (0.62–0.64 V at 0.2 A cm^{-2}, 160 °C) with similar acid doping levels [40]. Additionally, these values are improved over the s-PBI/*p*-PBI random copolymer membranes prepared via the PPA process (0.599–0.663 V at 0.2 A cm^{-2}, 160 °C, composition dependent) [41]. These results are vastly improved over previous literature reports of water-doped sulphonated PBI membranes. Staiti et al. [56] tested post-sulphonated *m*-PBI in a hydrogen/oxygen (3 bar/5 bar) fuel cell from 80 to 120 °C with humidified gases. The high OCV (0.9 V) was promising, but the voltage immediately decreased to zero when a load was applied to the cell. Bae et al. tested a propylsulphonate-

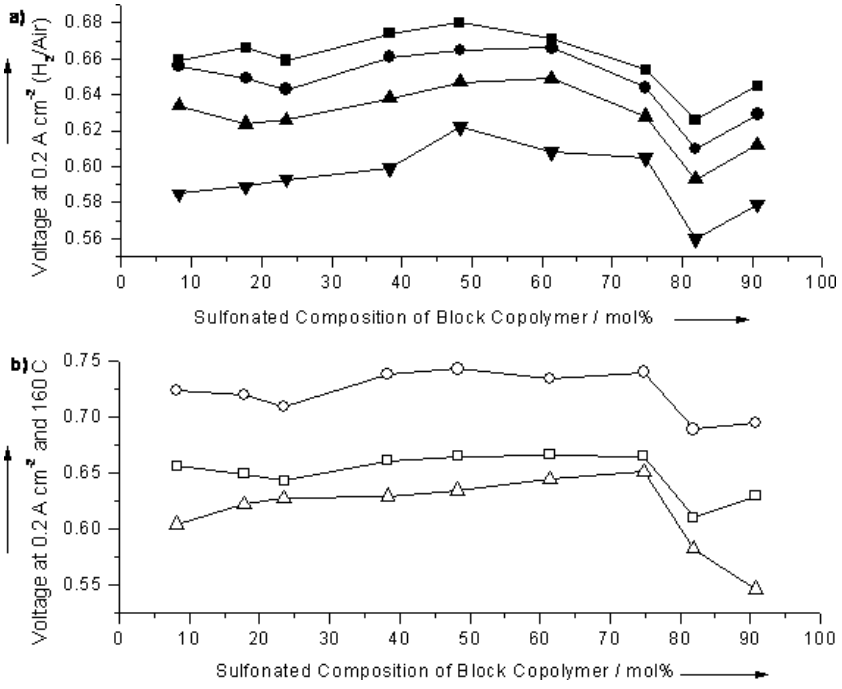

Fig. 4 s-PBI/p-PBI segmented block copolymer fuel cell performance with (a) hydrogen–air at different temperatures (180 °C, squares; 160 °C, circles, 140 °C, triangle; 120 °C, inverted triangle) and (b) different fuels and oxidants at 160 °C (H_2–Air, open squares; H_2–O_2, open circles; Reformate–Air, open triangles).

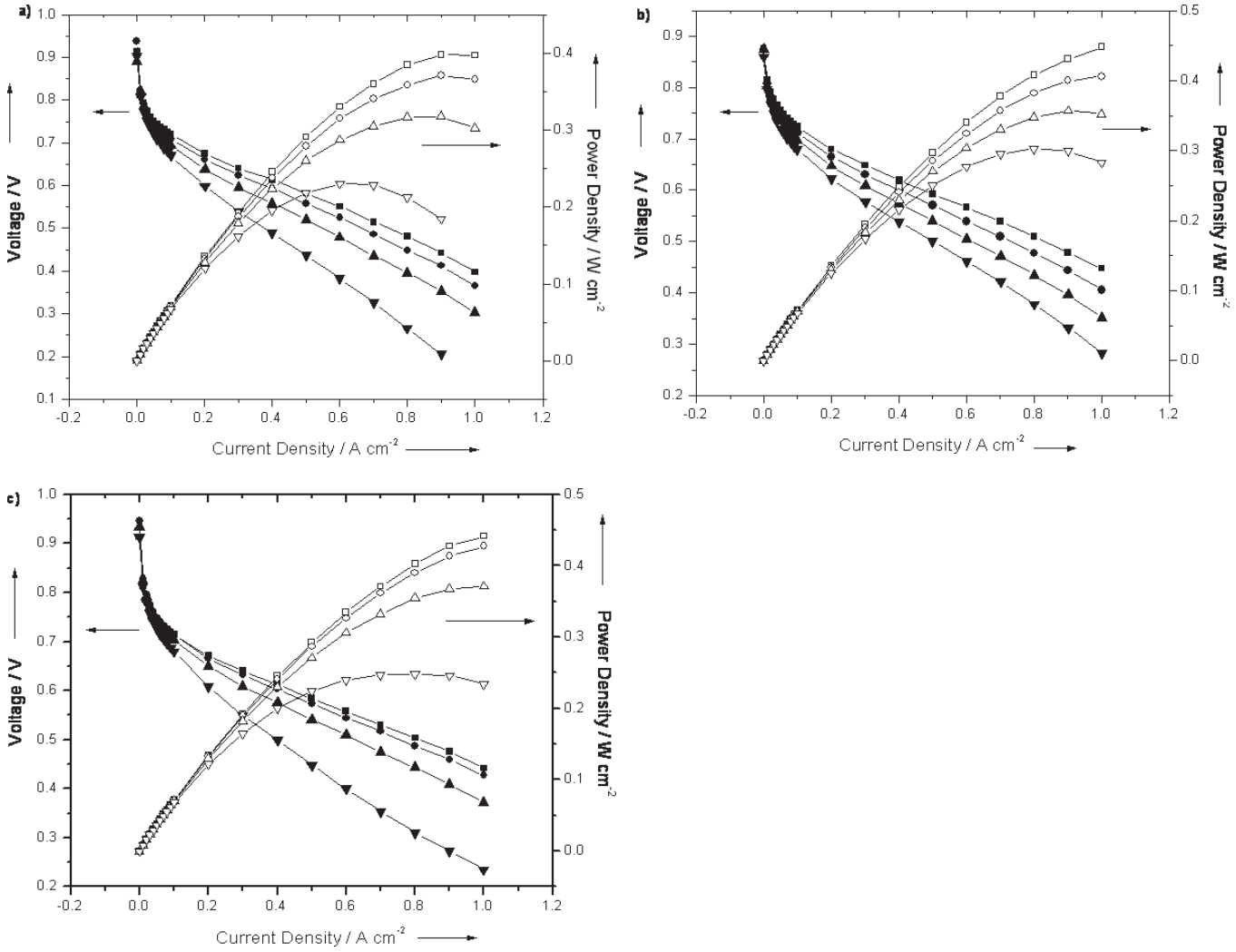

Fig. 5 Hydrogen–air fuel cell performance (180 °C, closed squares; 160 °C, closed circles; 140 °C, closed triangles; 120 °C, closed inverted triangles) and power density curves (180 °C, open squares; 160 °C, open circles; 140 °C, open triangles; 120 °C, open inverted triangles) for (a) 40/60 s-PBI/*p*-PBI segmented block copolymer, (b) 50/50 s-PBI/*p*-PBI segmented block copolymer and (c) 60/40 s-PBI/*p*-PBI segmented block copolymer.

grafted *m*-PBI in a humidified hydrogen/oxygen fuel cell at 80 °C. The performance was found to be ~0.45 V at 0.2 A cm^{-2} [60]. An MEA with 0.4 mg cm^{-2} Pt catalyst was prepared from the butylsulphonate-grafted *m*-PBI backbone. When tested under hydrogen/oxygen at 80 °C and ambient total pressure, 100% RH, the water-doped polymer showed a maximum performance of 0.2 W cm^{-2} at 0.7 A cm^{-2} (voltage equal to 0.29 V). The segmented block copolymers compare favourably to the other PBI chemistries produced via the PPA process [32, 33, 36–39] and show similar robust long-term performance.

The long-term performance of the s-PBI/*p*-PBI segmented block copolymers was excellent, even with multiple air starvation periods (Figure 6). The segmented block copolymers typically showed break-in periods (voltage increased until stabilisation) of ~ 200 h, likely due to the unoptimised pressing conditions used during MEA fabrication. The 40/60 s-PBI/*p*-PBI segmented block copolymers showed significantly lower break-in times (10 h), indicating that pressing conditions for these membranes were likely more suited to the polymer properties.

Remarkably, the membranes showed full or nearly full performance recovery even with multiple air starvation periods and station events caused by equipment failures. The 60/40 and 40/60 s-PBI/*p*-PBI segmented block copolymer membranes showed full recovery from all air starvation periods. The 50/50 s-PBI/*p*-PBI segmented block copolymer showed a performance loss of 33 mV after a 40 h starvation period and an additional decrease of 23 mV after a second 40 h starvation period. The unexplained station events had a greater immediate effect on fuel cell performance than air starvation. After experiencing a station event, the 60/40 s-PBI/*p*-PBI segmented block copolymer membrane initially lost 0.1527 V at 0.2 A cm^{-2}, but recovered over ~ 100 h with only a 2 mV performance decrease compared to preevent. In general, however, the overall recovery from both air starvation and unexplained losses of cell operation for the segmented block copolymers indicate the robustness and excellent durability

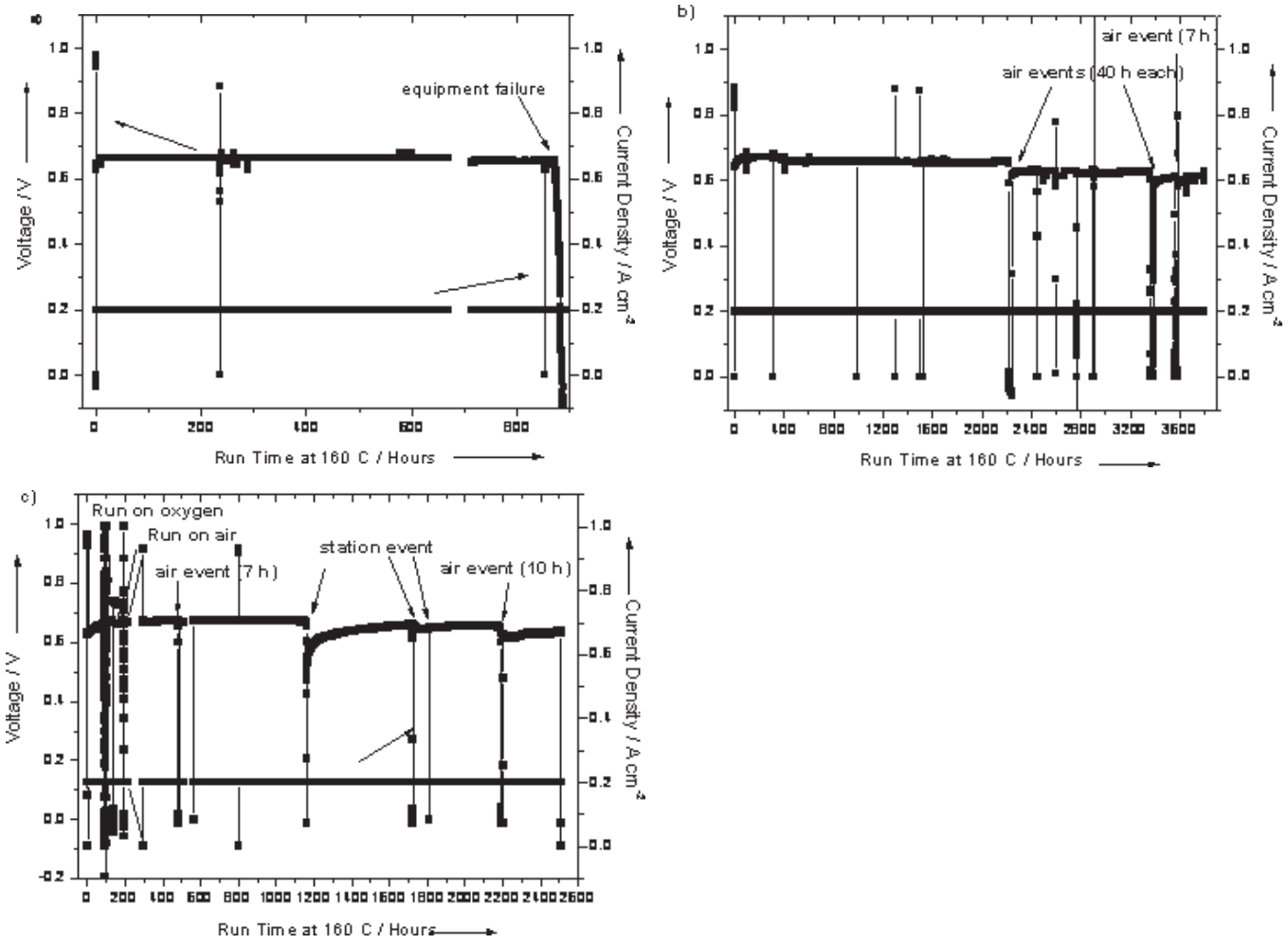

Fig. 6 Long-term hydrogen–air performance at 160 °C and 0.2 A cm^{-2} for (a) 40/60 s-PBI/*p*-PBI segmented block copolymer, (b) 50/50 s-PBI/*p*-PBI segmented block copolymer and (c) 60/40 s-PBI/*p*-PBI segmented block copolymer.

of the block copolymer membranes for fuel cell operation even under extreme conditions.

3.4.2 *Hydrogen–Oxygen Fuel Cell Performance*

Fuel cell performance for all segmented block copolymers was improved by using oxygen instead of air as the oxidant, as seen in Figure 7. The highest performance was observed for the 50/50 s-PBI/*p*-PBI membrane, with a voltage of 0.742 V at 0.2 A cm^{-2} and 160 °C. The 40/60 and 60/40 s-PBI/*p*-PBI membranes had similar performances of 0.738 and 0.734 V, respectively. There were some mass transport limitations for the cathode, as observed from the tailing at high-current densities in some of the hydrogen–air polarisation curves in Figure 5. The mass transport limitations were eliminated by switching to oxygen, and performance at the higher current densities was excellent. Using the Nernst Equation, the expected performance gain when switching from air to oxygen at 160 °C is ~65 mV. The segmented block copolymers showed improvements of 66–96 mV, depending on composition. The 50/50 and 40/60 s-PBI/*p*-PBI block copolymers showed higher than expected improvements (77 mV). This is likely due to the unoptimised pressing conditions during MEA fabrication. If overcompression occurs during the pressing process, some of the polymer membrane can be forced into the electrodes, coating the catalyst particles with polymer or blocking the gas channels. If this happens, the diffusion times of fuel or oxidant to the catalyst surface are much longer, especially when the concentration of the reactant gas is decreased (i.e. reformate *vs.* hydrogen or air *vs.* oxygen). This would explain the greater than theoretical increases when switching from air (21% oxygen) to pure oxygen gases. The hydrogen–oxygen performance of these membranes is significantly improved compared to the sulphonated hydrocarbon-based membranes in the literature, and to typical acid-doped (non-sulphonated) *m*-PBI membranes.

Wang et al. [47] tested non-sulphonated *m*-PBI that had been doped in 5 M Pa in a humidified H_2/O_2 fuel cell at 150 °C for 200 h. The cell was held at a constant cell voltage of 0.55 V with almost no performance loss and robust fuel cell performance. Li et al. [24] reported fuel cell performance of acid-doped *m*-PBI cells run with non-humidified H_2/O_2

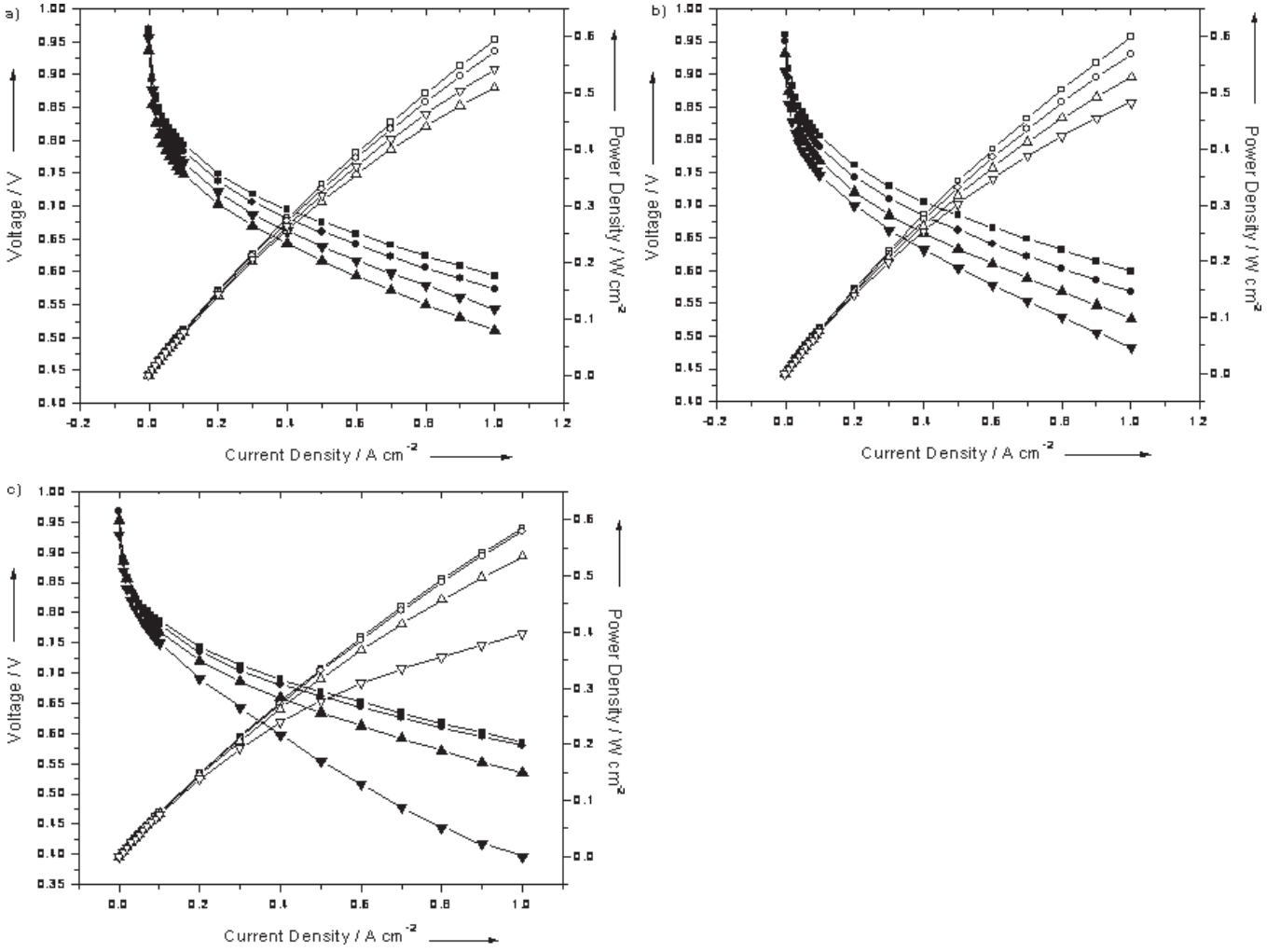

Fig. 7 Hydrogen–oxygen fuel cell performance (180 °C, closed squares; 160 °C, closed circles; 140 °C, closed triangles; 120 °C, closed inverted triangles) and power density curves (180 °C, open squares; 160 °C, open circles; 140 °C, open triangles; 120 °C, open inverted triangles) for (a) 40/60 s-PBI/*p*-PBI segmented block copolymer, (b) 50/50 s-PBI/*p*-PBI segmented block copolymer and (c) 60/40 s-PBI/*p*-PBI segmented block copolymer.

(3 bar/3 bar). At 200 °C, the maximum performance was 1.0 W cm^{-2}; however, the doping level of the PBI membrane was not reported. A 10 cm^2 cell with Pt catalyst loading of 0.5 mg cm^{-2} was run on H_2/O_2 with a hydrogen flow rate of 30 mL min^{-1} cm^{-2} and achieved ~0.65 V at 0.2 A cm^{-2} at 100 °C. Long-term current density monitoring was performed at 120 °C for 3 500 h and 150 °C for 5000 h, with a steady state voltage of 0.5 V over these test periods. Savinell et al. [67] tested a 5 mol PA/PRU doped non-sulphonated *m*-PBI membrane with humidified H_2/O_2 and methanol/O_2 at 150 °C. The E-TEK electrodes had Pt loading of 0.5 mg cm^{-2} and these cells showed a maximum performance with H_2/O_2 of 0.25 W cm^{-2} at 0.700 A cm^{-2}, or 0.357 V at this current density. The cell was also operated continuously for 200 h at 0.2 A cm^{-2} with no performance decreases. In comparison, the block copolymers show voltages of 0.623, 0.622 and 0.627 V at 0.700 A cm^{-2} for the 40/60, 50/50 and 60/40 s-PBI/*p*-PBI membranes, respectively. This is a ~0.27 V improvement under similar conditions, using non-humidified gases.

3.4.3 *Reformate–Air Performance*

The reformate–air performance of the segmented block copolymers was poor compared to hydrogen–air for all compositions, as seen in Figure 8. The highest performance was seen for the 60/40 s-PBI/*p*-PBI segmented block copolymer with a voltage of 0.644 V at 0.2 A cm^{-2} and 160 °C, followed by the 50/50 and 40/60 s-PBI/*p*-PBI copolymers, with voltages of 0.638 and 0.634 V, respectively. Performance improved with increasing temperature, as expected from the Nernst Equation. The lower reformate performance, especially at temperatures below 160 °C, was likely due to competitive binding of the carbon monoxide impurity to the Pt catalyst. However, performance is lower than would be expected due only to catalyst poisoning. To determine if there was an irreversible reaction occurring on the catalyst surface, leading to decreased performance, a reformate recovery study was undertaken. The fuel cell was held at different temperatures (180, 160, 140 and 120 °C) with reformate–air feeds for 8 h before changing to the next temperature. The results of this

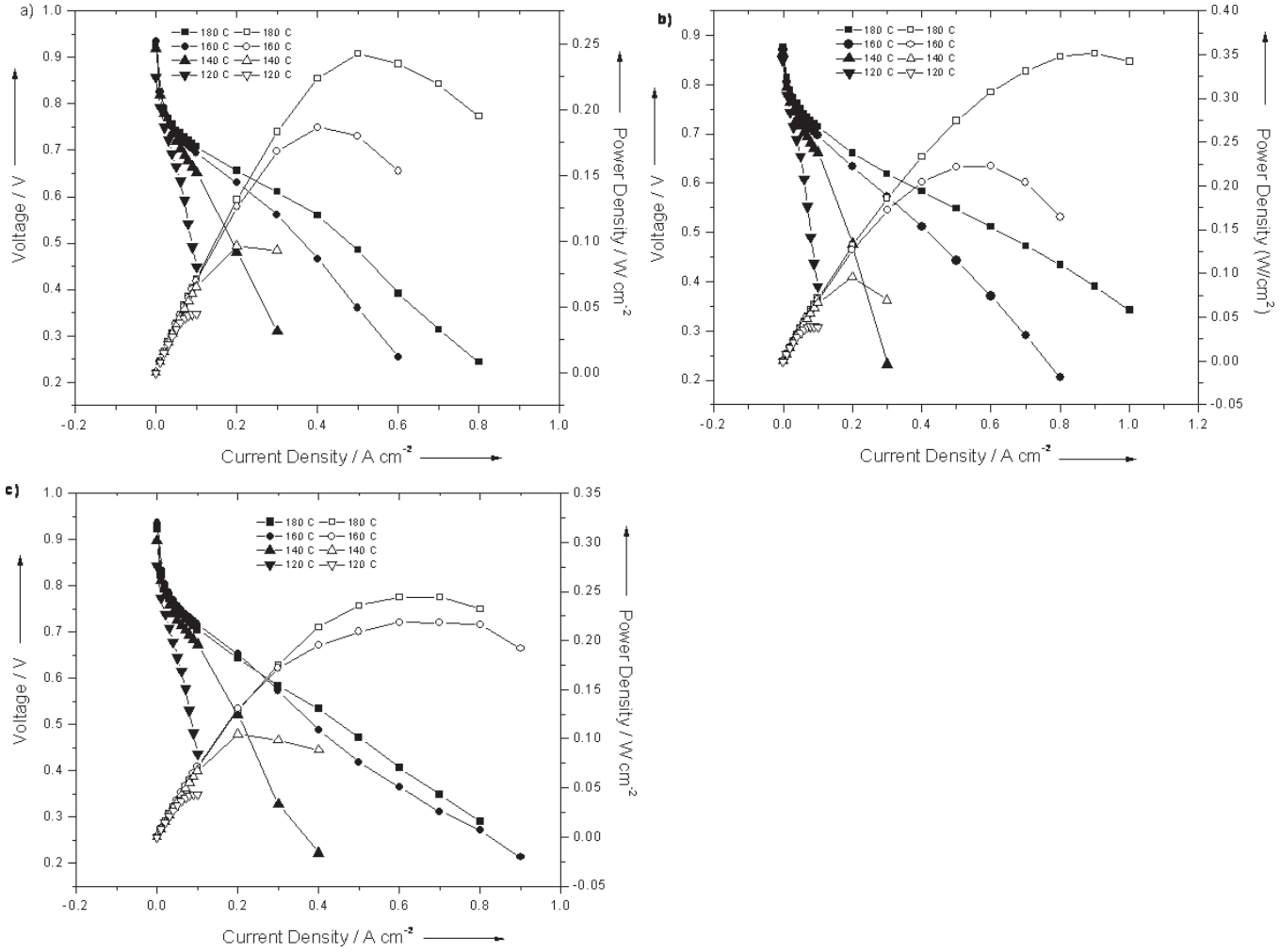

Fig. 8 Reformate–air fuel cell performance (180 °C, closed squares; 160 °C, closed circles; 140 °C, closed triangles; 120 °C, closed inverted triangles) and power density curves (180 °C, open squares; 160 °C, open circles; 140 °C, open triangles; 120 °C, open inverted triangles) for (a) 40/60 s-PBI/*p*-PBI segmented block copolymer, (b) 50/50 s-PBI/*p*-PBI segmented block copolymer and (c) 60/40 s-PBI/*p*-PBI segmented block copolymer.

study are shown in Figure 9. The performance at 180 and 160 °C were typical of reformate–air for s-PBI-based membranes, while performance at 140 °C was significantly lower as the CO–Pt binding affected cell performance. When the temperature was lowered to 120 °C, the cell could not maintain a constant current of 0.2 A cm^{-2} and ceased operating for the 8 h of testing. Upon switching back to hydrogen and 160 °C, nearly complete recovery of the cell voltage was seen (0.662 V before reformate, 0.646 V immediately after switching to hydrogen and 0.656 V after 1 h of hydrogen). These data indicate that any effects of CO on the Pt catalyst were completely reversible by returning to higher temperatures and pure hydrogen and there was no long-term negative effect on cell performance over the lifetime.

3.4.4 Fuel Cell Performance Comparisons

Because no clear correlations could be made among the segmented block copolymers with respect to increasing s-PBI content, the performance was compared to the homopolymers and random copolymer of the same composition (50/50 s-PBI/*p*-PBI). The hydrogen–air, hydrogen–oxygen, reformate–air (160 °C) and conductivity curves are shown in Figure 10. It was observed that the s-PBI homopolymer had the lowest performance with hydrogen–air. The 50/50 s-PBI/*p*-PBI random copolymer showed improved performance over the s-PBI homopolymer, and the 50/50 s-PBI/*p*-PBI block copolymer had better performance than either the homopolymer or random copolymer. The *p*-PBI homopolymer showed slightly improved performance over the other polymers tested, with the differences being more notable at the higher current densities.

The hydrogen–oxygen performance differences were smaller, likely due to the higher amount of oxidant gas present. With more oxygen present than in air, starvation was prevented and diffusion to the catalyst particles coated by the polymer membrane, as discussed previously, was improved. The *p*-PBI homopolymer and 50/50 s-PBI/*p*-PBI block copolymer showed nearly identical performances when tested with hydrogen–oxygen. The s-PBI homopolymer per-

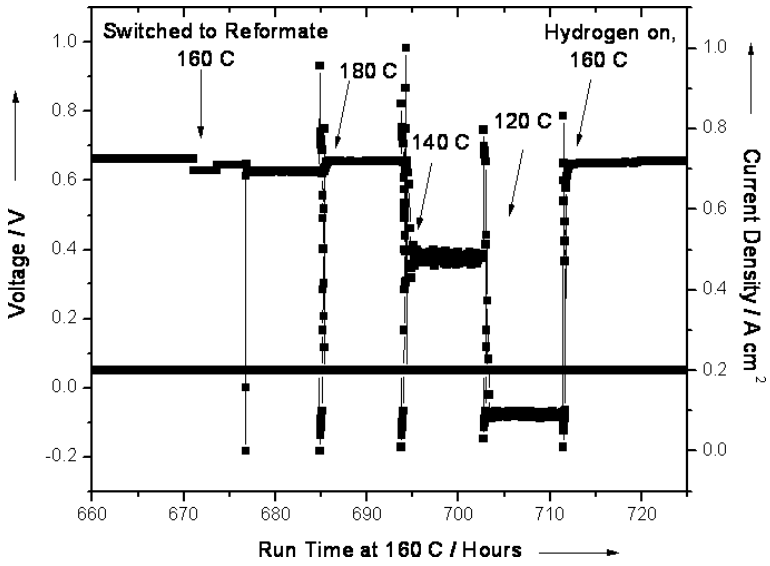

Fig. 9 Reformate recovery study of the 40/60 s-PBI/*p*-PBI segmented block copolymer. The cell was run for 8 h at each temperature with reformate gas, then hydrogen gas was used as the fuel at 160 °C.

formance was slightly decreased over these two polymers, while the 50/50 s/*p*-PBI random copolymer showed significantly decreased performance, especially at higher current densities.

The reformate–air performance was highest for the *p*-PBI homopolymer except at higher current densities. The 50/50 s-PBI/*p*-PBI block copolymer has slightly lower performance than *p*-PBI until a current density of 0.7 A cm^{-2}. At this current density, the performances were the same and the block copolymer was able to maintain voltage to 0.8 A cm^{-2} while the *p*-PBI homopolymer was not. The 50/50 s-PBI/*p*-PBI block copolymer reformate–air performance was significantly improved over the s-PBI homopolymer at all current densities tested, with greater gains seen at higher current densities. While the reformate–air performances are lower than the hydrogen–air values, the block copolymer still shows excellent performance with a reduced hydrogen flow and in the presence of a carbon monoxide impurity.

The conductivities of the four polymers are shown in Figure 10d. The unoptimised 50/50 s-PBI/*p*-PBI random copolymer showed the lowest conductivity (0.148 S cm^{-1} at 180 °C), while the *p*-PBI homopolymer showed the highest conductivity at 180 °C (0.344 S cm^{-1}). Interestingly, the conductivity of the block copolymer was higher than the *p*-PBI homopolymer until 120 °C, where the values were equivalent. The block copolymer conductivity was excellent at 180 °C (0.329 S cm^{-1}), and was improved over the highly optimised s-PBI homopolymer (0.279 S cm^{-1}). While the block and random copolymers showed slightly lower conductivities than the *p*-PBI homopolymer, the application of a new sulphonated PBI chemistry in combination with a novel synthetic method (the PPA process) was able to produce a not yet optimised series of membranes that show radically improved conductivities compared to the previously produced similar chemistries of PA-doped sulphonated hydrocarbon-based polymers in the literature.

4 Conclusions

A series of high-molecular weight segmented block copolymers of s-PBI and *p*-PBI were successfully prepared via a two-step method using the PPA process. The reaction time and conditions were highly important for producing high-molecular weight stable gel films and the initial IV value of the prepolymers had a great effect on final film forming properties. All molar ratios of s-PBI to *p*-PBI yielded robust gel films under appropriate synthesis and hydrolysis conditions. There were no direct correlations between s-PBI content and membrane properties for acid doping, conductivity and mechanical properties. The fuel cell membrane properties, while not showing correlations, were all extremely high. However, moderate incorporation of s-PBI into the copolymer (40–60 mol%) showed the best balance of fuel cell membrane properties. The acid loading levels, conductivity and mechanical properties were improved over the s-PBI homopolymer and random copolymers of s-PBI and *p*-PBI for similar compositions, and comparable to the *p*-PBI homopolymer. The membrane properties were significantly improved over the few reports of PBI block copolymers in the literature. In general, increasing s-PBI content in the block copolymer led to lower IV values, lower conductivity (>75 mol%), increased modulus and increased weight loss during TGA at 425–525 °C.

Detailed studies on fuel cell performance with different fuels and oxidants were conducted and showed excellent performance for all compositions, even after multiple air starvation periods and station disruptions. The highest performance was observed for polymers with 40–60 mol% s-PBI in the segmented block copolymers, though all copolymer compositions showed excellent voltage outputs. The higher performance for polymers with moderate s-PBI and *p*-PBI ratios was likely due to a balance of polymer molecular weight, mechanical properties, acid loading and conductivity, all of which contribute to fuel cell performance. Additionally, the highest amount of block copolymer morphology would be seen at these moderate mole ratios. Performance for the best segmented block copolymer (50/50 s-PBI/*p*-PBI, Figure 10) was comparable to *p*-PBI and significantly higher than the s-PBI homopolymer and random copolymers of similar compositions, likely due to the different architecture of block copolymers *versus* random copolymers. As can be seen in our previous work [41], a random copolymer morphology improved fuel cell performance and membrane properties over the s-PBI homopolymer. The addition of the block copolymer morphology to the novel sulphonated polymer allows for further property and performance improvements. Most copolymers showed excellent long-term durability and

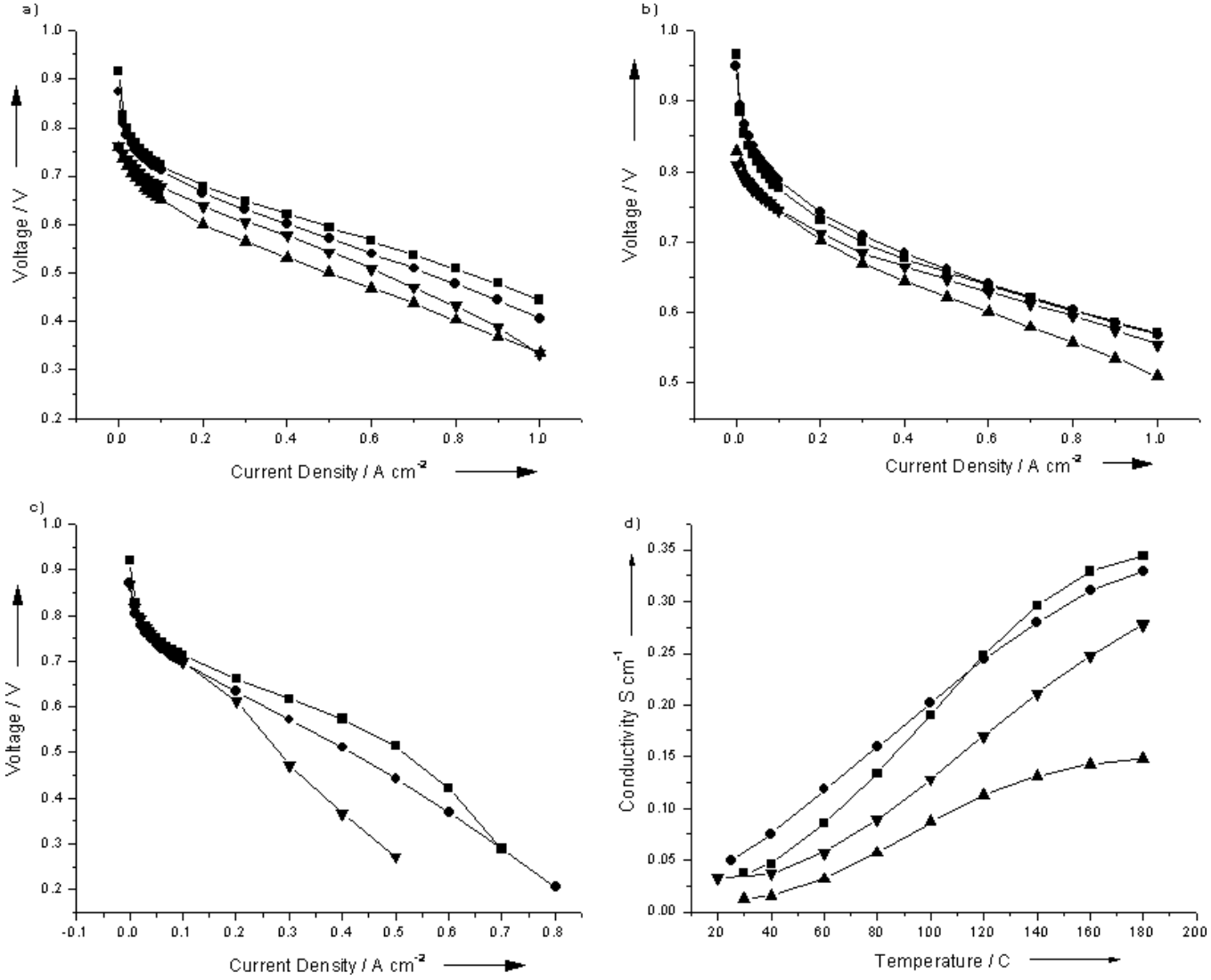

Fig. 10 Fuel cell performance and proton conductivity comparisons of the s-PBI (▼) and p-PBI (■) homopolymers with the 50/50 s-PBI/p-PBI random copolymer (▲) and 50/50 s-PBI/p-PBI block copolymer (●) for (a) hydrogen–air (160 °C); (b) hydrogen–oxygen (160 °C); (c) reformate–air (160 °C); and (d) proton conductivity at different temperatures.

performance recovery even after multiple starvation periods and station events.

Acknowledgement

The authors would like to thank BASF Fuel Cell, Inc. for their generous support during the course of this work.

References

[1] B. C. H. Steele, A. Heinzel, *Nature* **2001**, *414*, 345.
[2] T. A. Zawodzinski, T. E. Springer, J. Davey, R. Jestel, C. Lopez, J. Valerio, S. Gottesfeld, *J. Electrochem. Soc.* **1993**, *140*, 1981.
[3] Q. Li, R. He, J. O. Jensen, N. J. Bjerrum, *Chem. Mater.* **2003**, *15*, 4896.
[4] S. Faure, R. Mercier, P. Aldebert, M. Pineri, B. Sillon, *French Patent 9605707* **1996**.
[5] T. Watari, J. Fang, K. Tanaka, H. Kita, K.-I. Okamoto, T. Hirano, *J. Membr. Sci.* **2004**, *230*, 111.
[6] F. Lufrano, I. Gatto, P. Staiti, V. Antonucci, E. Passalacqua, *Solid State Ionics* **2001**, *145*, 47.
[7] B. R. Einsla, W. L. Harrison, C. Tchatchoua, J. E. McGrath, *Polym. Prepr.* **2004**, *44*, 645.
[8] M. Gil, X. Ji, X. Li, H. Na, J.E. Hampsey, Y. Lu, *J. Membr. Sci.* **2004**, *234*, 75.
[9] P. Xing, G. P. Robertson, M. D. Guiver, S. D. Mikhailenko, S. Kaliaguine, *Macromolecules* **2004**, *37*, 7960.
[10] X. Jin, M. T. Bishop, T. S. Ellis, F. E. Karasz, *Br. Polym. J.* **1985**, *17*, 4.
[11] Y. Gao, G. P. Robertson, M. D. Guiver, S. D. Mikhailenko, S. Kaliaguine, *Macromolecules* **2004**, *37*, 6748.

[12] F. Wang, M. Hickner, Y. S. Kim, T. A. Zawodzinski, J. E. McGrath, *J. Membr. Sci.* **2002**, *197*, 231.
[13] G. Y. Xiao, G. M. Sun, D. Y. Yan, P. F. Zhu, P. Tao, *Polym. Prepr.* **2002**, *43*, 5335.
[14] M. A. Hickner, H. Ghassemi, Y. S. Kim, B. R. Einsla, J. E. McGrath, *Chem. Rev.* **2004**, *104*, 4587.
[15] S. Kim, D. A. Cameron, Y. Lee, J. R. Reynolds, C. R. Savage, *J. Polym. Sci. Part A: Polym. Chem.* **1996**, *34*, 481.
[16] H. R. Allcock, E. C. Kellam III, M. A. Hofmann, *Macromolecules* **2001**, *34*, 5140.
[17] H. R. Allcock, R. J. Fitzpatrick, L. Salvati, *Chem. Mater.* **1991**, *3*, 1120.
[18] P. M. Blonsky, D. F. Shriver, P. Austin, H. R. Allcock, *J. Am. Chem. Soc.* **1984**, *106*, 6854.
[19] K. Miyatake, H. Iyotani, K. Yamamoto, E. Tsuchida, *Macromolecules* **1996**, *29*, 6969.
[20] P. Jannasch, *Curr. Opin. Colloid Interface Sci.* **2003**, *8*, 96.
[21] H. G. Herz, K. D. Kreuer, J. Maier, G. Scharfenberger, M. F. H. Schuster, W. H. Meyer, *Electrochim. Acta* **2003**, *48*, 2165.
[22] K. D. Kreuer, A. Fuchs, M. Ise, M. Spaeth, J. Maier, *Electrochim. Acta* **1998**, *43*, 1281.
[23] M. Schuster, W. H. Meyer, G. Wegner, H. G. Herz, M. Ise, K. D. Kreuer, J. Maier, *Solid State Ionics* **2001**, *145*, 85.
[24] Q. Li, R. He, J. O. Jensen, N. J. Bjerrum, *Fuel Cells* **2004**, *4*, 147.
[25] Y. S. Kim, F. Wang, M. Hickner, T. A. Zawodzinski, J. E. McGrath, *J. Membr. Sci.* **2003**, *212*, 263.
[26] P. Donoso, W. Gorecki, C. Berthier, F. Defendini, C. Poinsignon, M. B. Armand, *Solid State Ionics* **1988**, *28*, 969.
[27] S. Petty-Weeks, J. J. Zupanicic, J. R. Swedo, *Solid State Ionics* **1988**, *31*, 117.
[28] D. Rodriguez, C. Jegat, O. Trinquet, J. Grondin, J. C. Lassegues, *Solid State Ionics* **1993**, *61*, 195.
[29] J. R. Stevens, W. Wieczorek, D. Raducha, K. R. Jeffrey, *Solid State Ionics* **1997**, *97*, 347.
[30] W. Wieczorek, J. R. Stevens, *Polymer* **1997**, *38*, 2057.
[31] R. Tanaka, H. Yamamoto, A. Shono., K. Kubo, M. Sakurai, *Electrochim. Acta* **2000**, *45*, 1385.
[32] G. Qian, B. C. Benicewicz, *J. Polym. Sci., Part A: Polym. Chem.* **2009**, *47*, 4064.
[33] G. Qian, D. W. Smith, B. C. Benicewicz, *Polymer* **2009**, *50*, 3911.
[34] J. Mader, L. Xiao, T. Schmidt, B. C. Benicewicz, In *Advances in Polymer Science, Special Vol. Fuel Cells*, (Ed. G. Scherer) Springer-Verlag: Berlin, **2008**, pp. 63.
[35] J. S. Wainright, J. T. Wang, D. Weng, R. F. Savinell, M. Litt, *J. Electrochem. Soc.* **1995**, *142*, L121.
[36] L. Xiao, H. Zhang, E. Scanlon, L. S. Ramanathan, E. W. Choe, D. Rogers, T. Apple, B. C. Benicewicz, *Chem. Mater.* **2005**, *17*, 5328.
[37] L. Xiao, H. Zhang, T. Jana, R. Chen, E. Scanlon, E. W. Choe, L. S. Ramanathan, S. Yu, B. C. Benicewicz, *Fuel Cells* **2005**, *5*, 287.
[38] S. Yu, B. C. Benicewicz, *Macromolecules* **2009**, *42*, 8640.
[39] S. Yu, H. Zhang, L. Xiao, E.-W. Choe, B.C. Benicewicz, *Fuel Cells* **2009**, *9*, 318.
[40] J. A. Mader, B. C. Benicewicz, *Macromolecules* **2010**, *43*, 6706.
[41] J. A. Mader, B. C. Benicewicz, *Fuel Cells* **2011**, *11 (2)*, 212.
[42] R. He, Q. Li, G. Xiao, N. J. Bjerrum, *J. Membr. Sci.* **2003**, *226*, 169.
[43] D. Weng, J. S. Wainright, U. Landau, R. F. Savinell, *J. Electrochem. Soc.* **1996**, *143*, 1260.
[44] S. R. Samms, S. Wasmus, R. F. Savinell, *J. Electrochem. Soc.* **1996**, *143*, 1225.
[45] R. F. Savinell, M. H. Litt, *US Patent, US 973796*, **1997**.
[46] R. F. Savinell, M. H. Litt, *US Patent US 9613872*, **1996**.
[47] J. T. Wang, J. S. Wainright, R. F. Savinell, M. Litt, H. Yu, *Electrochim. Acta* **1996**, *41*, 193.
[48] H. Bai, W. S. W. Ho, *J. Taiwan Inst. Chem. Eng.* **2009**, *40*, 260.
[49] J. Peron, E. Ruiz, D. J. Jones, J. Roziere, *J. Membr. Sci.* **2008**, *314*, 247.
[50] X. Glipa, M. El Haddad, D. J. Jones, J. Roziere, *Solid State Ionics* **1997**, *97*, 323.
[51] M. J. Ariza, D. J. Jones, J. Roziere, *Desalination* **2002**, *147*, 183.
[52] H. Xu, K. Chen, X. Guo, J. Fang, J. Yin, *Polymer* **2007**, *28*, 5556.
[53] J. A. Asensio, S. Borros, P. Gomez-Romero, *J. Polym. Sci. Part A: Polym. Chem.* **2002**, *40*, 3703.
[54] J. Jouanneau, R. Mercier, L. Gonon, G. Gebel, *Macromolecules* **2007**, *40*, 983.
[55] M. Rikukawa, K. Sanui, *Prog. Polym. Sci.* **2000**, *25*, 1463.
[56] P. Staiti, F. Lufrano, A. S. Arico, E. Passalacqua, V. Antonucci, *J. Membr. Sci.* **2001**, *188*, 71.
[57] S. Qing, W. Huang, D. Yan, *Eur. Polym. J.* **2005**, *41*, 1589.
[58] Z. Bai, G. E. Price, M. Yoonessi, S. B. Juhl, M. F. Durstock, T. D. Dang, *J. Membr. Sci.* **2007**, *305*, 69.
[59] K. A. Perry, *Ph.D. Thesis,* Rensselaer Polytechnic Institute, Troy, NY, USA **2009**.
[60] J. M. Bae, I. Honma, M. Murata, T. Yamamoto, M. Rikukawa, N. Ogata, *Solid State Ionics* **2002**, *147*, 189.
[61] D. J. Jones, J. Roziere, *J. Membr. Sci.* **2001**, *185*, 41.
[62] H. Bai, W. S. W. Ho, *Ind. Eng. Chem.* **2009**, *48*, 2344.
[63] H. Pu, Q. Liu, *Polym. Int.* **2004**, *53*, 1512.
[64] M. Kawahara, M. Rikukawa, K. Sanui, *Polym. Adv. Technol.* **2000**, *11*, 544.
[65] J. Larminie, A. Dicks, *Fuel Cell Systems Explained*. *2nd ed.*; John Wiley & Sons Ltd, England, **2003**.
[66] EG&G Technical Services, I., *Fuel Cell Handbook*. 6th ed.; U.S. Department of Energy under contract no. DE-AM26-99FT40575: 2002.
[67] R. F. Savinell, E. Yeager, D. Tryk, U. Landau, J. S. Wainright, D. Weng, K. Lux, M. Litt, C. Rogers. *J. Electrochem. Soc.* **1994**, *141*, L46.

